Conceptualizing Ribosomal mRNA Unwinding Utilizing DMS MaP-Seq

Preston A. Kellenberger[1], Peter V. Cornish[1]

1 Department of Biochemistry, University of Missouri, Columbia, MO, USA

Abstract

Examining the dynamicity of RNA structure has deepened our understanding of its vast biological functions. Perhaps the protein complex that encounters the most diverse landscape of RNA structure is the ribosome. In translation, the ribosome must linearize countless mRNA conformations for proper protein production. Some RNA structures, however, reliably make up sequences which hinder the ability of the ribosome to maintain its reading frame. Arguably, the most well-studied of these structures is the RNA pseudoknot. Here, we present an approach utilizing dimethyl sulfate probing with mutational profiling and sequencing (DMS MaP-Seq) to precisely examine RNA unwinding. DMS MaP-Seq is a method typically used in predicting RNA secondary structure. Instead, we employ the method to understand the unfolding of the Sugarcane Yellow Leaf Virus pseudoknot ($ScYLV_{PK}$). We demonstrate that the unwinding of $ScYLV_{PK}$ is inherently different with regards to the ribosome and temperature. Additionally, we find that minor-groove triplex interactions support coaxial stacking, providing a major source of stability to $ScYLV_{PK}$ in ribosomal unwinding.

Introduction

In translation, the ribosome can only interpret single-stranded RNA to allow proper codon-tRNA alignment. However, complex intramolecular RNA secondary/tertiary structures are commonplace in transcripts. These structures, then, must be linearized before the bacterial ribosome is able to read their corresponding nucleotides. Central in aiding linearization of mRNA within bacteria is the ribosomal helicase center composed of proteins S3, S4, and S5 located within the 30S subunit [1]. Unlike DNA helicases such as DnaB, which are tasked only with unwinding the double helix conformation, S3, S4, and S5 must be able to unwind extensive combinations of RNA structure [2]. Fascinatingly, despite such vast modes of operation, it has been shown that these ribosomal helicase proteins do not require direct use of ATP or GTP [1]. Furthermore, little is understood about the underlying mechanical function of

proteins S3, S4, and S5. These unique attributes of the ribosomal helicase center, compounded with the dynamicity of the ribosome, make ribosomal unwinding a process of which much is unknown.

-1 programmed ribosomal frameshifting (-1 PRF) is a phenomenon that resides centrally within the uncertainties of mRNA unwinding. Due to evolutionary pressures on their relatively small genome, many viruses utilize -1 PRF as a means to produce multiple proteins from a single coding mRNA [3]. In -1 PRF, the ribosome slips out of the original reading frame by shifting one nucleotide backwards, producing a different polypeptide. Three components are necessary for -1 PRF to occur. A slippery sequence (X XXY YYZ where X is any nucleotide, Y is A or U, and Z is A, U, or C), a downstream stable structure (ex. *dnaX* hairpin, HIV-1 hairpin, luteoviral pseudoknots), and a linker/spacer sequence positioned between the previous two elements [4-6]. It has been demonstrated that the length of the linker sequence (which typically ranges from 5nt-9nt) is vital for substantial rates of frameshifting [7]. Many have demonstrated that the linker length needs to be short enough to provide tension between the ribosome and the downstream secondary structure, but not too short to where the ribosome has partially or completely unwound the structure before arriving at the slip site [8,9]. Preliminary studies speculated that the thermostability of secondary structures found in frameshifting capable RNAs would provide resistance to the ribosome. However, it is now known that the Tm of the mRNA has no correlation on frameshifting efficiency [10-12]. Therefore, the intricate unfolding patterns of these mRNA structures are fundamentally linked to their interaction with the ribosome, which is crucial for understanding how the ribosome processes mRNA and influences frameshifting efficiency.

Starting nearly three decades ago, a wide array of experimental approaches have been employed to understand the unwinding of mRNA pseudoknots. Initially, differential scanning calorimetry and UV-vis thermal denaturation experiments were employed [13-18]. These studies sufficiently determined the global unfolding mechanisms of many RNA pseudoknots but were unable to examine precise nucleotide-level changes. Additionally, they provided limited information on the 3-dimensional structure of the RNA, results which could greatly inform a PRF mechanism. X-ray crystallography and NMR experiments overcame these barriers through atomic resolution of many pseudoknots [19-27]. However, similar to thermodynamic studies, the effectiveness of these approaches are limited in the presence of the ribosome. Force

measurements have also been used in unwinding experiments, measured directly through nanopores, or indirectly through tweezers. Tweezer experiments provided information about macro-molecular unwinding of the RNA, indicating an order of denaturing interactions. However, these experiments lack precision and sensitivity, suggesting singular intermediate structures in unwinding [10,12,28-32]. Additionally, force is applied to either end of the RNA to establish tension in the transcript, a factor extraneous to translation. Nanopores attempt to mimic the ribosomal mRNA entry tunnel by pulling mRNA through the channel while reading blocking signatures, indicating possible unfolding states [33]. Nanopores, however, present imprecise unfolding intermediates similar to that of tweezers. Additionally, all the above methods fail to consider how the complexity and dynamicity of the ribosome affect unwinding of RNA pseudoknots. In an effort to overcome this barrier, mutational experiments have speculated regions of the pseudoknots that may provide stability by analyzing the relative frameshifting efficiencies and thermodynamic stabilities [11,34,35]. Recently, tweezer experiments have been performed in the presence of the ribosome [36-38]. Examining the effects of ribosomal presence with tweezers produces a more accurate depiction of unwinding; however, the results still suffer from imprecision and extraneous 3' forces. Cryo-electron microscopy structures of early-stage ribosome/pseudoknot interaction have been released, but are only able to image well defined states, leading to difficulty in visualizing the heterogeneous partially-unwound RNA [39]. Probing techniques, such as RNases or dimethyl sulfate (DMS), permitted nucleotide-level precision in their results, but were traditionally limited in sensitivity [14,40,5,41,42]. Despite the benefits and limitations of these approaches, the need to examine ribosomal unwinding with nucleotide level-precision persisted.

While DMS probing has traditionally been used in RNA structure determination, our research applies the technique to RNA unwinding. In a traditional DMS experiment, RNA secondary structure can be deduced by analyzing which nucleotides are or are not modified by the chemical probe. Due to the recent developments in deep sequencing technologies, DMS probing has become a much more powerful tool. DMS mutational profiling and sequencing (DMS MaP-Seq) allows for high throughput data collection by the sequencing of modified oligonucleotides [43]. Due to the sequencing of millions of reads, the results are highly precise and can expose quantifiable and smaller changes in reactivity as compared to the traditional DMS probing approach, which relies on gel analysis [43]. The amount of experimental freedom is

another highlight for the use of DMS MaP-Seq. Whereas many approaches substitute the ribosome's unwinding force, the simultaneous use of DMS MaP-Seq with the ribosome requires little additional effort beyond setting up ribosome/mRNA constructs. Furthermore, adding tRNAs and elongation factors in DMS MaP-Seq experiments allow for the investigation of ribosomal state as it pertains to mRNA probe reactivity [44]. In a 2009 study, Mazauric et. al used DMS probing in the presence/absence of the ribosome on the beet western yellow virus pseudoknot ($BWYV_{PK}$) [41]. In these experiments, ribosomal unwinding of $BWYV_{PK}$ was investigated by stalling ribosomes upstream (11-12 nucleotides from the P site) of the RNA structure. We sought to expand the scope of these experiments by utilizing DMS MaP-Seq and by leveraging multiple ribosomal states. In the attempts to elucidate how these mRNAs are unwound, we have chosen the Sugarcane Yellow Leaf Virus (ScYLV) pseudoknot as the basis of our experimentation. The ScYLV pseudoknot ($ScYLV_{PK}$) has been well characterized in multiple studies and its structure has been solved through NMR [23,24]. Additionally, the wild-type $ScYLV_{PK}$ contains a larger frameshifting efficiency than that of BWYV [24,41]. However, as is the case with $ScYLV_{PK}$ and all other mRNA structures found within frameshifting cassettes, little is known about how the RNA is unwound in the process of translation.

In the following experiments, we employ the first use of DMS MaP-Seq on a ribosome-mRNA complex to provide a comprehensive look at ribosomal unwinding of $ScYLV_{PK}$. Our findings demonstrate that ribosomal unwinding is highly dependent on both the ribosome's positional distance from the pseudoknot and tRNA occupancy. Specifically, minor-groove triplex interactions and the helical junction were identified as critical elements stabilizing $ScYLV_{PK}$ during ribosomal unwinding. Additionally, our results reveal distinct differences between the unwinding effects of the ribosome and temperature, emphasizing the unique mechanisms by which the ribosome interacts with structured RNA. These insights advance our understanding of how ribosomal site occupancy may influence RNA stability and frameshifting efficiency, offering a refined framework to study RNA unwinding.

Results

Probing thermal unwinding of $ScYLV_{PK}$.

Previous research suggests that the thermostability of nucleic acid structures found in frameshifting sequences (FSS) have no correlation to the frameshifting efficiency [10-12]. Thermal denaturation experiments using differential scanning calorimetry (DSC) and UV-vis spectrophotometry determined the global unfolding characteristics of many FSS [13-18]. These experiments infer unfolding mechanisms only equipped with information on the entire molecule, and not individual residues. In this study, we sought to examine the unfolding of $ScYLV_{PK}$ with nucleotide-level precision using DMS MaP-Seq. For the following experiments, we constructed an mRNA to investigate the thermal unwinding of $ScYLV_{PK}$ and interactional changes due to the ribosome. Our 84 nt mRNA contains a ribosomal binding site, AUG and UUU codons for tRNA binding, +11 linker sequence (see "Ribosomal state changes pseudoknot unfolded state"), $ScYLV_{PK}$, and a trailing sequence (Figure 1). To determine the specific interactions involved in the thermal unwinding of $ScYLV_{PK}$, we incubated the RNA at 20˚C, 25˚C, 30˚C, and 35˚C in the absence of the ribosome. After the incubation period (see Materials and Methods), DMS was added to the solution. In this time, DMS methylates A and C nucleotides at Watson-Crick positions (N1 and N3 respectively) and N7 of G [45]. Although many factors contribute to the modification rate of a given nucleotide, Watson-Crick interactions and hydrogen bonding reliably reduce the probability of modification. Reverse transcription of the RNA promotes mutation at methylated nucleotides (although less reliable for G) [46]. Through deep sequencing, we measured the mutational frequency of each individual nucleotide within $ScYLV_{PK}$ to generate a mutational profile.

To produce the above color map (Figure 2A), we calculated and plotted changes in reactivity of $ScYLV_{PK}$ as compared to a mutational profile of the RNA at 20˚C, anticipating that it would demonstrate greater stability than the elevated temperatures. In traditional DMS MaP-Seq experiments, the secondary structure of an RNA is determined through SHAPE data, an output from DMS MaP-Seq analysis. For our experiments, we wanted to determine changes in RNA stability, since the structure of $ScYLV_{PK}$ has already been determined [23]. To focus on small and precise flexibility changes, we instead handled the mutational frequency at each nucleotide. As the temperature of the sample increases from 20˚C to 25˚C,

marginal increases in reactivity are observed near the terminal stem 2 (S2) nucleotides of the pseudoknot. In the 30˚C construct, additional interactions near the helical junction (G7 through C14) show increased reactivity to DMS. At 35˚C, stem 1 (S1) interactions (A3 through G7) exhibit increased flexibility in addition to the preceding interactions mentioned in the 25˚C and 30˚C constructs. Our observed temperature-dependent progressive molecular destabilization agrees with global molecular models of RNA pseudoknot unfolding [13,14,35]. While the intrinsic activity of DMS increases with temperature, we observe a non-uniform distribution of reactivity increases across $ScYLV_{PK}$. Such a pattern indicates that the reactivity differences are not substantially directed by temperature-dependent DMS activity, but rather from macro-molecular destabilization of the RNA [47].

Ribosomal state changes pseudoknot unfolded state.

One critical element within FSS is the length of the linker sequence. Typically, 5-9nt linker sequence lengths are necessary to induce frameshifting [9]. Linker sequences of this length place the RNA structure at the helicase center of the ribosome, which resides +11nt from the 5' residue in the bacterial ribosomal P site [1,7]. Arginine- and lysine-rich helicase proteins (S3, S4, and S5) occupy the helicase center and are thought to interact with the phosphodiester backbone of the transcript [1]. A select few studies have attempted to examine ribosomal unwinding of RNA, but, due to technique limitations, are unable to observe nucleotide-level changes [36-38]. Additionally, it has been observed that -1 frameshifting efficiency drops sharply when the downstream structural element is positioned further than +13 from the ribosomal P site [9]. Considering these parameters, we constructed +11 and +12 ScYLV RNAs to investigate changes in ribosomal unwinding. The RNAs are identical except for the addition of uracil between A2 and A3 (Figure 1). This addition places the structure +12nt from the stalled ribosomal P site as opposed to +11nt (Figure 1).

In addition to studying $ScYLV_{PK}$ with respect to ribosomal distance, we also sought to determine the effect of P/A site occupancy. It has been found that the addition of A – site tRNA causes the ribosomal entry tunnel to constrict 1-3 Å, an effect which may play a role in both intersubunit rotation and unwinding [48]. As reported from previous smFRET data, the ribosomal state can be manipulated via the addition of

tRNAs, elongation factors, GTP, and other various reaction components [44,49]. The classical and hybrid states define the ratcheting motion of the translating ribosome. In previous fluorescence studies, we have identified an additional state of hyper rotation [49]. The hyper rotated state appears to form when the ribosome is within close proximity to a downstream nucleic acid structure [50]. Additionally, this state appears to arise from hybrid state ribosomes assuming further counterclockwise rotation. Consequently, the current uncertainty in the rotational state prompted us to focus our terminology on site occupancy. To maintain accuracy in our descriptions, we will be referring to our experimental conditions with the following notation: acylated P – site tRNA (aP-tRNA) (traditionally shifts equilibrium to the classical state), deacylated P – site tRNA (daP-tRNA) (traditionally shifts equilibrium to the hybrid state), and daP-tRNA with acylated A – site tRNA to construct the pre-translocation state (PRE).

To understand the effect of ribosomal state on $ScYLV_{PK}$ in our +11 and +12 systems, we obtained mutational profiles from the aP-tRNA, daP-tRNA, and PRE states. From these mutational profiles, we wanted to determine the effect the ribosome had on intramolecular $ScYLV_{PK}$ interactions. To find this, we first scaled the mutational frequencies of each experiment to limit the effect of fluctuations in universal modification rate. Our reference for calculating a scaling factor (S) was the 3' terminal adenosine in our data collection. This nucleotide is not involved within $ScYLV_{PK}$ structure, and therefore should not change in reactivity. We then multiplied S to each mutational frequency across the rest of the molecule:

$$S = \frac{f_{ref}}{f_{exp}} \qquad M_{scaled,n} = M_{exp,n}S$$

where S = scaling factor, f = reference mutational frequency, f = experimental mutational frequency, M = targeted experimental values, n = nucleotide.

Next, we calculated the mutational frequency difference from a modified RNA in the absence of the ribosome. The mutational differences were then normalized through calculation of a Z-score for each nucleotide. Each Z-score was calculated through comparing the reaction difference at each individual nucleotide across each state (aP-tRNa, daP-tRNA, and PRE):

$$Z = (X - \mu)/\sigma$$

where X = nucleotide reactivity difference, μ = mean of cross-experimental reactivity difference, and σ = standard deviation of cross-experimental reactivity difference.

We have found that the use of Z-score normalization produces a more accurate reference for nucleotide change from construct to construct. Additionally, one issue DMS MaP-Seq experiments present is the need to produce all experiments on the same day to limit extraneous reactivity changes [51]. Fluctuations in probe efficacy, reverse transcription, and reverse transcription buffer all can affect the ability to compare experiments to one another. We have found that through our normalization process, one can utilize reference mutational profiles from different days to produce similar results (Figure S1). Subsequent mapping of the mutational difference Z-scores generated color maps (Figure 3A, Figure 4).

Within our +11 system (Figure 3A), it can be observed that the aP-tRNA and daP-tRNA ribosomal states share similar trends in DMS reactivity, or nucleotide stability/flexibility. One large-sweeping similarity is that nucleotides near the helical junction (G7 through C14) and S2-associated triplex nucleotides (C27/C28) are less accessible to the probe, and thus are more stable. Destabilization, or increases in normalized DMS reactivity change, occurs within the first A-U base pairing in S1, and throughout much of loop 2 (L2), including adenosines involved in triplex interactions. Although these observations present similarities between both states, there are a few differences between the aP-tRNA and daP-tRNA states. Generally, it can be observed that stabilized interactions appear to be slightly stronger in magnitude in the daP-tRNA state as compared to the aP-tRNA state within G7 through C14. While the daP-tRNA and aP-tRNA states produce similar trends in changes of DMS reactivity with respect to each other, the probing the PRE construct reveals dramatic changes in $ScYLV_{PK}$. Particularly, residues C27 and C28 involved in minor-groove triplex interactions near the helical junction show the largest change in normalized reactivity difference as compared to the daP-tRNA construct (Figure 5), flipping from highly protected to highly flexible. Additionally, C14, which is involved in triplex base paring with C27, is much more reactive in PRE as compared to the aP-tRNA and daP-tRNA states. Overall, within our +11 system, we note a significant dependence of $ScYLV_{PK}$ DMS reactivity on ribosomal state. In contrast to our temperature-dependent experiments, a clear difference is visible from ribosomal unwinding of $ScYLV_{PK}$.

Next, we sought to determine the effects of ribosomal presence on $ScYLV_{PK}$ within the +12 RNA. After exposing the +12 RNA to the ribosome in the aP-tRNA, daP-tRNA, and PRE states, we again determined the reactivity change Z-scores (Figure 4). Our results show that when the ribosome is placed 1 nucleotide further away from $ScYLV_{PK}$, much of the resulting stability changes are lost as compared to +11, including residues C27/C28 (Figure 5). Aside from a select few sporadic increases in DMS reactivity, we observe near negligible changes in reactivity universally throughout the entire molecule regardless of ribosomal state. Thus, it is likely that the pseudoknot is no longer within range to produce observable unwinding effects. Decreased efficacy in unwinding correlating with ribosomal distance from the helicase center, is consistent with current models on ribosomal unwinding [1].

Discussion

In this study, we sought to identify sub-structural changes in $ScYLV_{PK}$ due to the ribosome and thermal denaturation using DMS MaP-Seq. Through the contrast of these changes, we aimed to identify the dynamic interactions of RNA pseudoknots, and factors influencing frameshifting efficiency. By probing $ScYLV_{PK}$ with respect to varying ribosomal parameters (distance and A/P site occupancy), we observed significant and precise changes within $ScYLV_{PK}$ stability.

Previously, we used smFRET to measure intersubunit rotation of stalled ribosomes. While the ribosome commonly occupies the well-defined hybrid and classical states, we have found that the presence of structured nucleic acid facilities the transition into a state of hyper-rotation, with the determinant factor being distance of the structural element to the ribosome [50]. In these experiments, only ribosomes placed with a linker distance of +11 and +12 exhibited populations of ribosomes in hyper-rotation. While we used the same ribosomes (E. *coli,* MRE600) as employed in this previous study, different FSS have varying optimal positioning of the ribosome from the structural element for maximal frameshifting efficiency [8,9]. Equipped with this information, we sought to determine how the structure of an RNA pseudoknot might change at these two relevant distances. Our color maps (Figure 3A, Figure 4)

indicate that the structure of $ScYLV_{PK}$ is dependent on ribosomal state to a much higher degree in the +11 system than in +12 system. Interestingly, within our previous fluorescence studies, +12 contains a reduced number of ribosomes in hyper-rotation (26%) as compared to +11 (43%) when encountering a frameshifting hairpin, *dnaX* [50].

In order to determine precise changes within $ScYLV_{PK}$ due to the ribosome, we probed the RNA under various states of ribosomal tRNA occupancy. Through finding differences in mutational rate from ribosome-bound experiments to that of a control in the absence of the ribosome, normalized alterations to nucleotide reactivity were determined. Interestingly, ribosomal presence in the aP-tRNA and daP-tRNA states resulted in strong stabilization of minor-groove tertiary interactions (S2/L1) and adjacent L1/S1 nucleotides near the helical junction (G7 through C14) (Figure 3A). aP-tRNA and daP-tRNA ribosomes also resulted in destabilization of major-groove triplex interactions and Watson-Crick paring within the first nucleotides of S1. Furthermore, minor-groove and their adjacent helical junction interactions seem to strengthen slightly in the daP-tRNA state (Figure 3A). The most dramatic changes occur when the ribosome assumes PRE. In the PRE state, we observe the destabilization near the helical junction (G7 through C14) coupled with dramatic destabilization of minor-groove triplex nucleotides (C27/28). In a previous study, we found that when the mutation C27A is introduced to ScYLV, frameshifting efficiency dropped from 15% to 2% even though the global conformation of both RNAs were essentially identical [24]. Fascinatingly, residues C27 and C28 exhibit the largest shifts in reactivity across these three probed states, exhibiting increased reactivity with respect to the control after strong stabilization (Figure 5). Thus, C27 and C28 are involved in hydrogen bonding that presents a large kinetic barrier to ribosomal unwinding of $ScYLV_{PK}$ as suggested in our previous study [24]. We propose that the helical junction is the key-contributor to placing the ribosome in a frameshifting-prone state, and that the coaxial stacking is maintained largely by minor-groove triplex interactions in $ScYLV_{PK}$.

One of our main objectives with these experiments was to expand upon the works of Mazauric et. al [41]. Previously, in their 2009 report, DMS probing was performed on $BWYV_{PK}$ in the presence and absence of the ribosome. They determined changes in DMS reactivity by comparing the band intensity of ribosome-bound RNA to ribosome-absent RNA. With the development of deep sequencing and DMS

MaP-Seq, we sought to determine a more sensitive and quantitative approach to probe ribosomal mRNA unwinding. Since Mazauric and colleagues only probed $BWYV_{PK}$ with ribosomes in the PRE state, we aimed to increase the number of tested ribosomal states (daP-tRNA and aP-tRNA) to better represent the dynamic nature of the ribosome. In contrast to the 2009 study which probed a frameshifting-capable (32-ΔG-BWYV) +11 RNA, our experiments focus on +11 RNA lacking a slip site. We believe that by removing the slip site, we can remove heterogeneity arising from frameshifted and non-frameshifted populations. With this approach, our probing data more accurately isolates the unwinding effects due to the ribosome. Our interpretations of ribosomal unwinding share some similarities and notable differences. In agreement with the 2009 study, our results show stabilization in tertiary interactions surrounding the helical junction at the back of S1 and L1, and destabilization near the front of S1. One notable difference in our results arises from reactivity changes in L2. While Mazauric et. al observe protection of the entire L2 region, we have found that most of L2 exhibits slight destabilization with sharp destabilization at the 3' terminus of L2 (C27/C28). The differences between our results may arise from the newfound sensitivity of MaP-Seq; however, it is also possible that $BWYV_{PK}$ is destabilized entirely differently by the ribosome, resulting in the reduced frameshifting efficiency as compared to $ScYLV_{PK}$ [23,41]. Indeed, the $BWYV_{PK}$ contains the equivalent of the $ScYLV_{PK}$ C27A mutation within the wild-type sequence, a factor we have speculated to previously reduce frameshifting efficiency [23].

While DMS MaP-Seq on the ribosomal-dependency of $ScYLV_{PK}$ can inform us of key interactions in unwinding, recontextualizing the data with thermal denaturation further accentuated these results. Through comparing the color maps of our +11 system and thermal denaturation (Figure 2, Figure 3), we observed that macromolecular $ScYLV_{PK}$ interactions are unwound in a different sequential order (Figure 6). When $ScYLV_{PK}$ is exposed to increasing temperature from 20˚C-35˚C, it appears as if all triplex interactions destabilize first, followed by the helical junction, and then S1 and S2. This model of unwinding aligns well with much of the early thermodynamic analyses performed on RNA pseudoknots [13,14]. In contrast, when the ribosome is bound to $ScYLV_{PK}$, strong stabilization is found near the helical junction and minor-groove base triples while major-groove base triples, L2, and the front of S1 are slightly destabilized. This stabilization near the helical junction, as the ribosome nears the pseudoknot, demonstrates the unique characteristics of ribosome/mRNA interactions. We believe these differences

demonstrate that the effect of unwinding due to the ribosome is inherently different to that of increasing temperature and explains the uncoupled nature of Tm to frameshifting efficiency.

As demonstrated in this study, the intricate RNA/RNA interactions within $ScYLV_{PK}$ are integral to understanding ribosomal unwinding. Our DMS MaP-Seq results paint a clearer picture of pseudoknot unwinding in the context of the field. Previous optical tweezer and mutational studies have suggested the importance of triplex interactions in accordance with unfolding resistance [30,35,52]. However, universal mechanical unfolding of RNA pseudoknots with tweezers is not correlated with frameshifting efficiency [30,52]. The selective stabilization of $ScYLV_{PK}$ minor-groove triplex interactions within our data explains the uncoupling of frameshifting efficiency to universal mechanical unfolding. However, the importance of individual triplex interactions are likely dependent upon the specific FSS, as some studies have found only major-groove interactions to promote frameshifting [30,53]. Additionally, many tweezer experiments present intermediate structures where entire stems/loops are completely unwound in one step [29-31]. Our work, however, serves to stand as a more precise method in determining how these intramolecular interactions change. Such information allows one not only to identify key nucleotide-level interactions in dynamic systems, but also the sequence of macro-molecular unwinding through the interrogation of varying ribosomal states. Within frameshifting constructs, the roles of the slippery site and linker sequence have been defined and well supported. Conversely, the mechanistic understanding of structural elements in frameshifting systems has been elusive. We believe that DMS Map-Seq provides a promising tool to investigate precise interactional changes in frameshifting RNAs arising from ribosomal presence.

With the first ever simultaneous use of DMS MaP-Seq with ribosome/mRNA constructs, we have leveraged the precision of the technique to elucidate how unique interactions within $ScYLV_{PK}$ change due to the ribosome. Our data exhibits that interactions within $ScYLV_{PK}$ are highly dependent upon the distance and tRNA occupancy of the ribosome. Simultaneously, the ribosomal effects on $ScYLV_{PK}$ are distinctly different than thermal denaturation alone. Thus, our understanding of ribosomal unwinding will advance more efficiently when the effects of the ribosome are considered. Despite advances, the role of RNA pseudoknots in FSS is still not fully understood. Ribosomal frameshifts may affect how the ribosome interacts with the structural element. Re-folding of a pseudoknot may place it in a non-native conformation

after a ribosome has translated through. Additionally, the RNA pseudoknots may influence the structural dynamics of the ribosome. Further investigation is required to answer much of the above items in order to paint a clearer picture of ribosomal frameshifting.

Methods and Materials

Construction and Purification of RNA and Ribosomes

Construction of a pUC19 vector plasmid containing the ScYLV sequence was carried out via sequence and ligation independent cloning (SLIC). Purification and digestion of the plasmid with EcoRV (NEB, R0195S) produced a linear DNA fragment containing the T7 promoter and ScYLV sequence (Supplementary Data). The DNA was then transcribed into mRNA via T7 RNA polymerase. Further isolation of the RNA was done through crush and soak purification [54]. Tight couple ribosomes (E. *coli,* MRE600) were purified as described by Staehelin and Maglott [55].

tRNA Preparation

$tRNA^{fMet}$ and $tRNA^{Phe}$ were purchased from MP Biomedicals and Sigma respectively.

Charging of the tRNA was done by the following: 4X methionine charging buffer (50mM Tris HCL pH 7.9, 150mM KCl, 7mM MgCl2, 0.1mM EDTA, 2.5mM ATP, 1mM DTT) or 4X phenylalanine charging buffer (100mM Tris HCL pH 7.9, 50mM KCl, 0.5mM EDTA, 2.5mM ATP, 1mM DTT) were mixed with tRNA (20µM final), phenylalanine (100µM final) or N10-formyl tetrahydrofolate (300µM final), 4X S100-tRNA extract (0.0125µL per pmol tRNA), and were incubated at 37˚C for 10 minutes. The reactions were quenched by the addition of 0.1 volumes of 3M NaOAc pH 5.2. Following phenol chloroform extraction, the samples were resuspended in MilliQ water to a final concentration of 40 µM. The samples were then run on a P6 column preequilibrated in 10 mM KOAC pH 6.1.

To acetylate Phe-tRNA^{Phe}, acetic anhydride was added to the sample. Following the addition of acetic anhydride, the sample was put on ice for 1 hour. The acetic anhydride and resting process was repeated an additional time. Then, following the addition of 2 volumes of 100% ethanol, the sample was transferred to a dry ice ethanol bath for 30 minutes. The tRNA was then spun down and run through a G25 spin column equilibrated in 1mM KOAc pH 5.3.

DMS Exposure

To ensure the RNA would assume the correct pseudoknot conformation, 10nM of ScYLV RNA was prepared via refolding in accordance with our previous studies of ScYLV [23,24]. For this, the RNA was heated to 60˚C for 5-10 minutes and then cooled on ice. 5X buffer was then added to the solution (250mM Tris pH 7.5, 500nM NH4Cl, 100mM MgCl2). Tight couple purified ribosomes (E. *coli,* MRE600) were added to the mix to a final concentration of 20nM, and samples were incubated at 37˚C for 5 minutes. tRNA (final concentration 30nM) was then added to a final reaction volume of 10µL, mixed, and incubated for 20-30 minutes at 37˚C.

After incubation, 15µL of 1X ribosomal buffer (50mM Tris pH 7.5, 100mM NH4Cl, 20mM MgCl2, 6mM BME) was added to the reaction, followed by the addition of 12µL of 1M bicine. Each reaction was then brought to the experimental temperature (20˚C, 25˚C, 30˚C, 35˚C, or 37˚C). 4µL of 1.7M DMS-Ethanol was added to the reaction tube and was incubated at their respective experimental temperature for 6 minutes. The reaction was quenched with the addition of 200µL of BME Stop Solution (BME, 2ng carrier RNA).

RNA Purification and Library Generation

To precipitate the RNA, 960ul of 100% ethanol and 1.5 µL glycogen was added to each reaction. The RNA was then precipitated at -80˚C, spun and washed with 100% ethanol three times, and resuspended in 50uL of RNAase free water. The resulting material was reverse transcribed (M-MLV RT) and purified (NEB Monarch DNA Cleanup Kit). Two rounds of PCR were used to tag each reaction with sequencing

barcodes (Illumina, Supporting Information). After verifying the length of the product on a gel, the samples were pooled and sequenced (Illumina NovaSeq 6000, 20M PE reads). The resulting data were analyzed via Shapemapper2 to obtain mutational profiles (Supporting Information).

Supporting Information:

Supplementary_Information: A document listing the sequences of the +11 and +12 RNAs and all primers used (PDF)

Supplemental_Figure_1: A color map of mutational difference Z-scores in +11 ScYLV with an alternative reference mutational profile (PDF)

DMS_Profiles: A folder containing raw shapemapper2 mutational frequency outputs (ZIP)

Acknowledgements:

We thank Dr. Zhenwei Song and Dr. Xiao Heng for providing us assistance with DMS MaP-Seq experimental protocol and data analysis. We thank the University of Kansas Medical Center – Genomics Core for generating the sequence data sets. The Genomics Core is supported by the Kansas Intellectual and Developmental Disabilities Research Center (NIH U54 HD 090216), the Molecular Regulation of Cell Development and Differentiation – COBRE (P30 GM122731), The NIH S10 High End Instrumentation Grant (NIH S10OD021743) and the Frontiers CTSA Grant (UL1TR002366). **Funding:** Mizzou Forward Undergraduate Research Training Grant, University of Missouri Agricultural Institute, and NSF: #2122902.

Figure Legends:

Figure 1: 2D representation of experimental RNA containing $ScYLV_{PK}$. Boxes surround location of ribosomal P site (AUG) and A site (UUU). "+1" above 5' P-site nucleotide is shown. *Symbols within $ScYLV_{PK}$ notate non-Watson-Crick interactions as identified by Leontis et. al [56]. "The arrow present at 5' end of $ScYLV_{PK}$ between adenosines indicates location of uracil addition to produce +12 RNA.*

Figure 2: Color map from DMS probing at various temperatures. A) Color map representing mutational frequency difference of each nucleotide within $ScYLV_{PK}$ across 25˚C, 30˚C, and 35˚C with respect to 20˚C. Uracil residues are shown in gray to indicate their inability to react with DMS. B) 25˚C, 30˚C, and 35˚C color map outputs displayed on 2-dimensional representations of $ScYLV_{PK}$ sequence.

Figure 3: Color map from DMS probing of +11 $ScYLV_{PK}$ bound by ribosomes with different tRNAs. A) Color map representing mutational frequency difference Z-scores of each nucleotide in +11 $ScYLV_{PK}$ in aP-tRNA, daP-tRNA, and PRE ribosomal states. Uracil residues are shown in gray to indicate their inability to react with DMS. B) +11 aP-tRNA, daP-tRNA, and PRE color map results displayed on 2-dimensional representations of $ScYLV_{PK}$ sequence.

Figure 4: Color map representing mutational frequency difference Z-scores of each nucleotide in +12 $ScYLV_{PK}$ in aP-tRNA, daP-tRNA, and PRE ribosomal states. Uracil residues are shown in gray to indicate their inability to react with DMS.

Figure 5: Mutational frequency difference Z-scores of nucleotides C27 and C28 across aP-tRNA, daP-tRNA, and PRE states in +11 (blue) and +12 (orange) RNAs displayed on a bar graph.

Figure 6: A schematic detailing the proposed unwinding of $ScYLV_{PK}$ due to temperature (left) and a translating ribosome (right). Larger arrows/bonds indicate strengthened interactions while smaller arrows/bonds indicate weakening interactions.

S1: Color map representing mutational frequency difference Z-scores of each nucleotide in +11 $ScYLV_{PK}$ in aP-tRNA, daP-tRNA, and PRE ribosomal states compared to an alternative reference mutational profile. Uracil residues are shown in gray to indicate their inability to react with DMS.

Ascension Codes:

E. coli ribosomal protein S3: P0A7V3, E. coli ribosomal protein S4: P0A7V8, E. coli ribosomal protein S5: P0A7W1, E. coli elongation factor G: P0A6M8.

References:

1. Takyar, S., Hickerson, R.P., and Noller, H.F. (2005). mRNA helicase activity of the ribosome. Cell *120*, 49-58.
2. Spinks, R.R., Spenkelink, L.M., Stratmann, S.A., Xu, Z.-Q., Stamford, N Patrick J., Brown, S.E., Dixon, N.E., Jergic, S., and van Oijen, A.M. (2021). DnaB helicase dynamics in bacterial DNA replication resolved by single-molecule studies. Nucleic Acids Research *49*, 6804-6816. 10.1093/nar/gkab493.
3. Chang, K.C., and Wen, J.D. (2021). Programmed -1 ribosomal frameshifting from the perspective of the conformational dynamics of mRNA and ribosomes. Comput Struct Biotechnol J *19*, 3580-3588. 10.1016/j.csbj.2021.06.015.
4. Chen, J., Petrov, A., Johansson, M., Tsai, A., O'Leary, S.E., and Puglisi, J.D. (2014). Dynamic pathways of -1 translational frameshifting. Nature *512*, 328-332. 10.1038/nature13428.
5. Mazauric, M.H., Seol, Y., Yoshizawa, S., Visscher, K., and Fourmy, D. (2009). Interaction of the HIV-1 frameshift signal with the ribosome. Nucleic Acids Res *37*, 7654-7664. gkp779 [pii]

10.1093/nar/gkp779.

6. Kim, H.K., and Tinoco, I., Jr. (2017). EF-G catalyzed translocation dynamics in the presence of ribosomal frameshifting stimulatory signals. Nucleic Acids Res *45*, 2865-2874. 10.1093/nar/gkw1020.
7. Napthine, S., Ling, R., Finch, L.K., Jones, J.D., Bell, S., Brierley, I., and Firth, A.E. (2017). Protein-directed ribosomal frameshifting temporally regulates gene expression. Nature Communications *8*, 15582. 10.1038/ncomms15582.
8. Volkenborn, K., Kuschmierz, L., Benz, N., Lenz, P., Knapp, A., and Jaeger, K.-E. (2020). The length of ribosomal binding site spacer sequence controls the production yield for intracellular and secreted proteins by Bacillus subtilis. Microbial Cell Factories *19*, 154. 10.1186/s12934-020-01404-2.
9. Lin, Z., Gilbert, R.J., and Brierley, I. (2012). Spacer-length dependence of programmed -1 or -2 ribosomal frameshifting on a U6A heptamer supports a role

for messenger RNA (mRNA) tension in frameshifting. Nucleic Acids Res *40*, 8674-8689. 10.1093/nar/gks629.
10. Chen, Y.-T., Chang, K.-C., Hu, H.-T., Chen, Y.-L., Lin, Y.-H., Hsu, C.-F., Chang, C.-F., Chang, K.-Y., and Wen, J.-D. (2017). Coordination among tertiary base pairs results in an efficient frameshift-stimulating RNA pseudoknot. Nucleic Acids Research *45*, 6011-6022. 10.1093/nar/gkx134.
11. Tholstrup, J., Oddershede, L.B., and Sørensen, M.A. (2012). mRNA pseudoknot structures can act as ribosomal roadblocks. Nucleic Acids Res *40*, 303-313. 10.1093/nar/gkr686.
12. Zhong, Z., Yang, L., Zhang, H., Shi, J., Vandana, J.J., Lam, D.T.U.H., Olsthoorn, R.C.L., Lu, L., and Chen, G. (2016). Mechanical unfolding kinetics of the SRV-1 gag-pro mRNA pseudoknot: possible implications for −1 ribosomal frameshifting stimulation. Scientific Reports *6*, 39549. 10.1038/srep39549.
13. Nixon, P.L., and Giedroc, D.P. (1998). Equilibrium unfolding (folding) pathway of a model H-type pseudoknotted RNA: the role of magnesium ions in stability. Biochemistry *37*, 16116-16129. 10.1021/bi981726z.
14. Qiu, H., Kaluarachchi, K., Du, Z., Hoffman, D.W., and Giedroc, D.P. (1996). Thermodynamics of Folding of the RNA Pseudoknot of the T4 Gene 32 Autoregulatory Messenger RNA. Biochemistry *35*, 4176-4186. 10.1021/bi9527348.
15. Theimer, C.A., and Giedroc, D.P. (1999). Equilibrium unfolding pathway of an H-type RNA pseudoknot which promotes programmed -1 ribosomal frameshifting. J Mol Biol *289*, 1283-1299. 10.1006/jmbi.1999.2850.
16. Nixon, P.L., Theimer, C.A., and Giedroc, D.P. (1999). Thermodynamics of stabilization of RNA pseudoknots by cobalt(III) hexaammine. Biopolymers *50*, 443-458. 10.1002/(SICI)1097-0282(19991005)50:4<443::AID-BIP9>3.0.CO;2-C.
17. Theimer, C.A., Wang, Y., Hoffman, D.W., Krisch, H.M., and Giedroc, D.P. (1998). Non-nearest neighbor effects on the thermodynamics of unfolding of a model mRNA pseudoknot. J Mol Biol *279*, 545-564. S0022-2836(98)91812-5 [pii]

10.1006/jmbi.1998.1812.
18. Wyatt, J.R., Puglisi, J.D., and Tinoco, I., Jr. (1990). RNA pseudoknots. Stability and loop size requirements. J Mol Biol *214*, 455-470. 10.1016/0022-2836(90)90193-p.
19. Pallan, P.S., Marshall, W.S., Harp, J., Jewett, F.C., Wawrzak, Z., Brown, B.A., Rich, A., and Egli, M. (2005). Crystal structure of a luteoviral RNA pseudoknot and model for a minimal ribosomal frameshifting motif. Biochemistry *44*, 11315-11322. 10.1021/bi051061i.
20. Su, L., Chen, L., Egli, M., Berger, J.M., and Rich, A. (1999). Minor groove RNA triplex in the crystal structure of a ribosomal frameshifting viral pseudoknot. Nature Structural Biology *6*, 285-292. 10.1038/6722.
21. Jones, C.P., and Ferré-D'Amaré, A.R. (2022). Crystal structure of the severe acute respiratory syndrome coronavirus 2 (SARS-CoV-2) frameshifting pseudoknot. Rna *28*, 239-249. 10.1261/rna.078825.121.
22. Frank, J., Zhu, J., Penczek, P., Li, Y., Srivastava, S., Verschoor, A., Radermacher, M., Grassucci, R., Lata, R.K., and Agrawal, R.K. (1995). A model of protein

synthesis based on cryo-electron microscopy of the E. coli ribosome. Nature *376*, 441-444. 10.1038/376441a0.
23. Cornish, P.V., Hennig, M., and Giedroc, D.P. (2005). A loop 2 cytidine-stem 1 minor groove interaction as a positive determinant for pseudoknot-stimulated -1 ribosomal frameshifting. Proc Natl Acad Sci USA *102*, 12694-12699. 10.1073/pnas.0506166102.
24. Cornish, P.V., Stammler, S.N., and Giedroc, D.P. (2006). The global structures of a wild-type and poorly functional plant luteoviral mRNA pseudoknot are essentially identical. RNA *12*, 1959-1969. 10.1261/rna.199006.
25. Holland, J.A., Hansen, M.R., Du, Z., and Hoffman, D.W. (1999). An examination of coaxial stacking of helical stems in a pseudoknot motif: the gene 32 messenger RNA pseudoknot of bacteriophage T2. Rna *5*, 257-271. 10.1017/s1355838299981360.
26. Shen, L.X., and Tinoco, I. (1995). The structure of an RNA pseudoknot that causes efficient frameshifting in mouse mammary tumor virus. J Mol Biol *247*, 963-978.
27. Puglisi, J.D., Wyatt, J.R., and Tinoco, I., Jr. (1990). Conformation of an RNA pseudoknot. J Mol Biol *214*, 437-453. 10.1016/0022-2836(90)90192-o.
28. Green, L., Kim, C.H., Bustamante, C., and Tinoco, I. (2008). Characterization of the mechanical unfolding of RNA pseudoknots. J Mol Biol *375*, 511-528. 10.1016/j.jmb.2007.05.058.
29. Hansen, T.M., Reihani, S.N., Oddershede, L.B., and Sørensen, M.A. (2007). Correlation between mechanical strength of messenger RNA pseudoknots and ribosomal frameshifting. Proc Natl Acad Sci USA *104*, 5830-5835. 10.1073/pnas.0608668104.
30. Chen, G., Chang, K.Y., Chou, M.Y., Bustamante, C., and Tinoco, I., Jr. (2009). Triplex structures in an RNA pseudoknot enhance mechanical stability and increase efficiency of -1 ribosomal frameshifting. Proc Natl Acad Sci U S A *106*, 12706-12711. 0905046106 [pii]

10.1073/pnas.0905046106.
31. Neupane, K., Zhao, M., Lyons, A., Munshi, S., Ileperuma, S.M., Ritchie, D.B., Hoffer, N.Q., Narayan, A., and Woodside, M.T. (2021). Structural dynamics of single SARS-CoV-2 pseudoknot molecules reveal topologically distinct conformers. Nat Commun *12*, 4749. 10.1038/s41467-021-25085-6.
32. Ritchie, D.B., Foster, D.A., and Woodside, M.T. (2012). Programmed -1 frameshifting efficiency correlates with RNA pseudoknot conformational plasticity, not resistance to mechanical unfolding. Proc Natl Acad Sci U S A *109*, 16167-16172. 10.1073/pnas.1204114109.
33. Zhang, X., Xu, X., Yang, Z., Burcke, A.J., Gates, K.S., Chen, S.J., and Gu, L.Q. (2015). Mimicking Ribosomal Unfolding of RNA Pseudoknot in a Protein Channel. J Am Chem Soc *137*, 15742-15752. 10.1021/jacs.5b07910.
34. Napthine, S., Liphardt, J., Bloys, A., Routledge, S., and Brierley, I. (1999). The role of RNA pseudoknot stem 1 length in the promotion of efficient −1 ribosomal frameshifting 11Edited by D. E. Draper. Journal of Molecular Biology *288*, 305-320. https://doi.org/10.1006/jmbi.1999.2688.

35. Kim, Y.G., Su, L., Maas, S., O'Neill, A., and Rich, A. (1999). Specific mutations in a viral RNA pseudoknot drastically change ribosomal frameshifting efficiency. Proc Natl Acad Sci U S A *96*, 14234-14239.
36. Desai, V.P., Frank, F., Lee, A., Righini, M., Lancaster, L., Noller, H.F., Tinoco, I., Jr., and Bustamante, C. (2019). Co-temporal Force and Fluorescence Measurements Reveal a Ribosomal Gear Shift Mechanism of Translation Regulation by Structured mRNAs. Molecular Cell *75*, 1007-1019.e1005. 10.1016/j.molcel.2019.07.024.
37. Qu, X., Wen, J.D., Lancaster, L., Noller, H.F., Bustamante, C., and Tinoco, I., Jr. (2011). The ribosome uses two active mechanisms to unwind messenger RNA during translation. Nature *475*, 118-121. nature10126 [pii]

10.1038/nature10126.
38. Qu, X., Lancaster, L., Noller, H.F., Bustamante, C., and Tinoco, I., Jr. (2012). Ribosomal protein S1 unwinds double-stranded RNA in multiple steps. Proc Natl Acad Sci U S A *109*, 14458-14463. 10.1073/pnas.1208950109.
39. Namy, O., Moran, S.J., Stuart, D.I., Gilbert, R.J., and Brierley, I. (2006). A mechanical explanation of RNA pseudoknot function in programmed ribosomal frameshifting. Nature *441*, 244-247. nature04735 [pii]

10.1038/nature04735.
40. Lund, P.E., Chatterjee, S., Daher, M., and Walter, N.G. (2019). Protein unties the pseudoknot: S1-mediated unfolding of RNA higher order structure. Nucleic Acids Research *48*, 2107-2125. 10.1093/nar/gkz1166.
41. Mazauric, M.H., Leroy, J.L., Visscher, K., Yoshizawa, S., and Fourmy, D. (2009). Footprinting analysis of BWYV pseudoknot-ribosome complexes. RNA *15*, 1775-1786. rna.1385409 [pii]

10.1261/rna.1385409.
42. Thulson, E., Hartwick, E.W., Cooper-Sansone, A., Williams, M.A.C., Soliman, M.E., Robinson, L.K., Kieft, J.S., and Mouzakis, K.D. (2020). An RNA pseudoknot stimulates HTLV-1 pro-pol programmed -1 ribosomal frameshifting. Rna *26*, 512-528. 10.1261/rna.070490.119.
43. Zubradt, M., Gupta, P., Persad, S., Lambowitz, A.M., Weissman, J.S., and Rouskin, S. (2017). DMS-MaPseq for genome-wide or targeted RNA structure probing in vivo. Nature Methods *14*, 75-82. 10.1038/nmeth.4057.
44. Cornish, P.V., Ermolenko, D.N., Noller, H.F., and Ha, T. (2008). Spontaneous intersubunit rotation in single ribosomes. Mol Cell *30*, 578-588. 10.1016/j.molcel.2008.05.004.
45. Krokhotin, A., Mustoe, A.M., Weeks, K.M., and Dokholyan, N.V. (2017). Direct identification of base-paired RNA nucleotides by correlated chemical probing. Rna *23*, 6-13. 10.1261/rna.058586.116.
46. Mitchell, D., 3rd, Cotter, J., Saleem, I., and Mustoe, A.M. (2023). Mutation signature filtering enables high-fidelity RNA structure probing at all four nucleobases with DMS. bioRxiv. 10.1101/2023.04.10.536308.
47. Rouskin, S., Zubradt, M., Washietl, S., Kellis, M., and Weissman, J.S. (2014). Genome-wide probing of RNA structure reveals active unfolding of mRNA structures in vivo. Nature *505*, 701-705. 10.1038/nature12894.

48. Jenner, L.B., Demeshkina, N., Yusupova, G., and Yusupov, M. (2010). Structural aspects of messenger RNA reading frame maintenance by the ribosome. Nat Struct Mol Biol *17*, 555-560. nsmb.1790 [pii]

10.1038/nsmb.1790.
49. Qin, P., Yu, D., Zuo, X., and Cornish, P.V. (2014). Structured mRNA induces the ribosome into a hyper-rotated state. EMBO Rep *15*, 185-190. 10.1002/embr.201337762.
50. Shebl, B., Pavlova, A., Kellenberger, P., Yu, D., Menke, D.E., Gumbart, J.C., and Cornish, P.V. (2024). The influence of downstream structured elements within mRNA on the dynamics of intersubunit rotation in ribosomes. bioRxiv, 2024.2010.2017.618931. 10.1101/2024.10.17.618931.
51. Liu, X., Huang, H., and Karbstein, K. (2022). Using DMS-MaPseq to uncover the roles of DEAD-box proteins in ribosome assembly. Methods *204*, 249-257. 10.1016/j.ymeth.2022.05.001.
52. Ritchie, D.B., Foster, D.A.N., and Woodside, M.T. (2012). Programmed −1 frameshifting efficiency correlates with RNA pseudoknot conformational plasticity, not resistance to mechanical unfolding. Proceedings of the National Academy of Sciences *109*, 16167-16172. doi:10.1073/pnas.1204114109.
53. Hsu, C.-F., Chang, K.-C., Chen, Y.-L., Hsieh, P.-S., Lee, A.-I., Tu, J.-Y., Chen, Y.-T., and Wen, J.-D. (2021). Formation of frameshift-stimulating RNA pseudoknots is facilitated by remodeling of their folding intermediates. Nucleic Acids Research *49*, 6941-6957. 10.1093/nar/gkab512.
54. Petrov, A., Wu, T., Puglisi, E.V., and Puglisi, J.D. (2013). Chapter Seventeen - RNA Purification by Preparative Polyacrylamide Gel Electrophoresis. In Methods in Enzymology, J. Lorsch, ed. (Academic Press), pp. 315-330. https://doi.org/10.1016/B978-0-12-420037-1.00017-8.
55. Staehelin, T., and Maglott, D.R. (1971). [47] Preparation of Escherchia coli ribosomal subunits active in polypeptide synthesis. In Methods in Enzymology, (Academic Press), pp. 449-456. https://doi.org/10.1016/S0076-6879(71)20049-5.
56. Leontis, N.B., Stombaugh, J., and Westhof, E. (2002). The non-Watson–Crick base pairs and their associated isostericity matrices. Nucleic Acids Research *30*, 3497-3531. 10.1093/nar/gkf481.

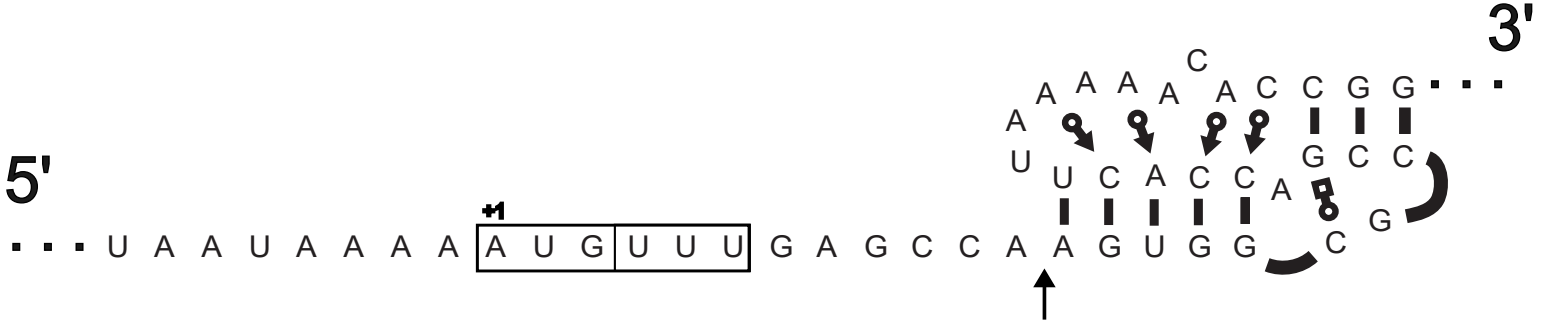
5'
3'
+1
U A A U A A A A A U G U U U G A G C C A A G U G G
A A A A A C C G G
U U C A C C A G C C
G C

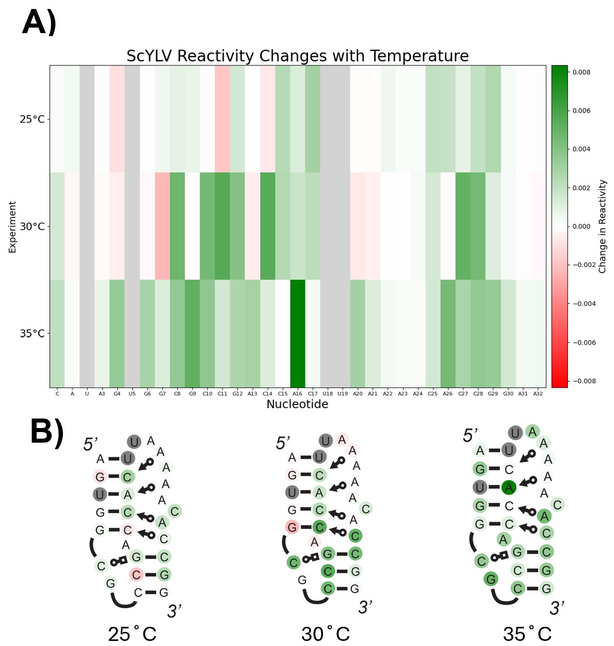
A)
ScYLV Reactivity Changes with Temperature
Experiment
25°C
30°C
35°C
Nucleotide
Change in Reactivity
0.008
0.006
0.004
0.002
0.000
−0.002
−0.004
−0.006
−0.008
B)
5'
3'
25˚C
30˚C
35˚C

Figure 2

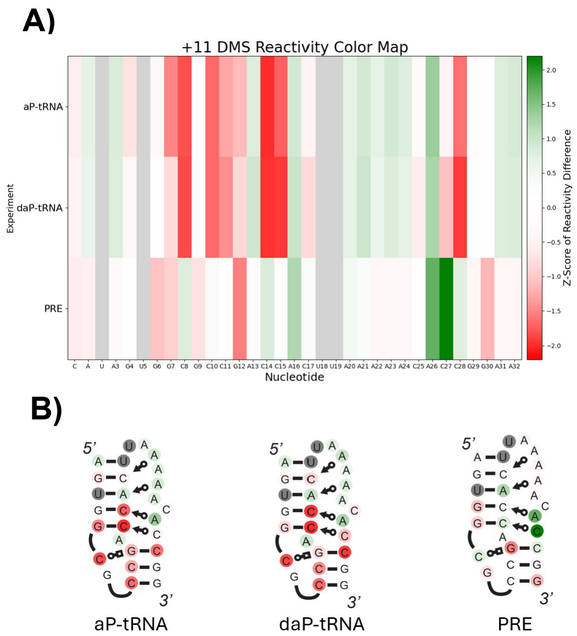
A)
+11 DMS Reactivity Color Map
aP-tRNA
daP-tRNA
PRE
Experiment
C A U A3 G4 U5 G6 G7 C8 G9 C10 C11 G12 A13 C14 C15 A16 C17 U18 U19 A20 A21 A22 A23 A24 C25 A26 C27 C28 G29 G30 A31 A32
Nucleotide
Z-Score of Reactivity Difference
2.0
1.5
1.0
0.5
0.0
−0.5
−1.0
−1.5
−2.0
B)
5'
3'
aP-tRNA
daP-tRNA
PRE

Figure 3

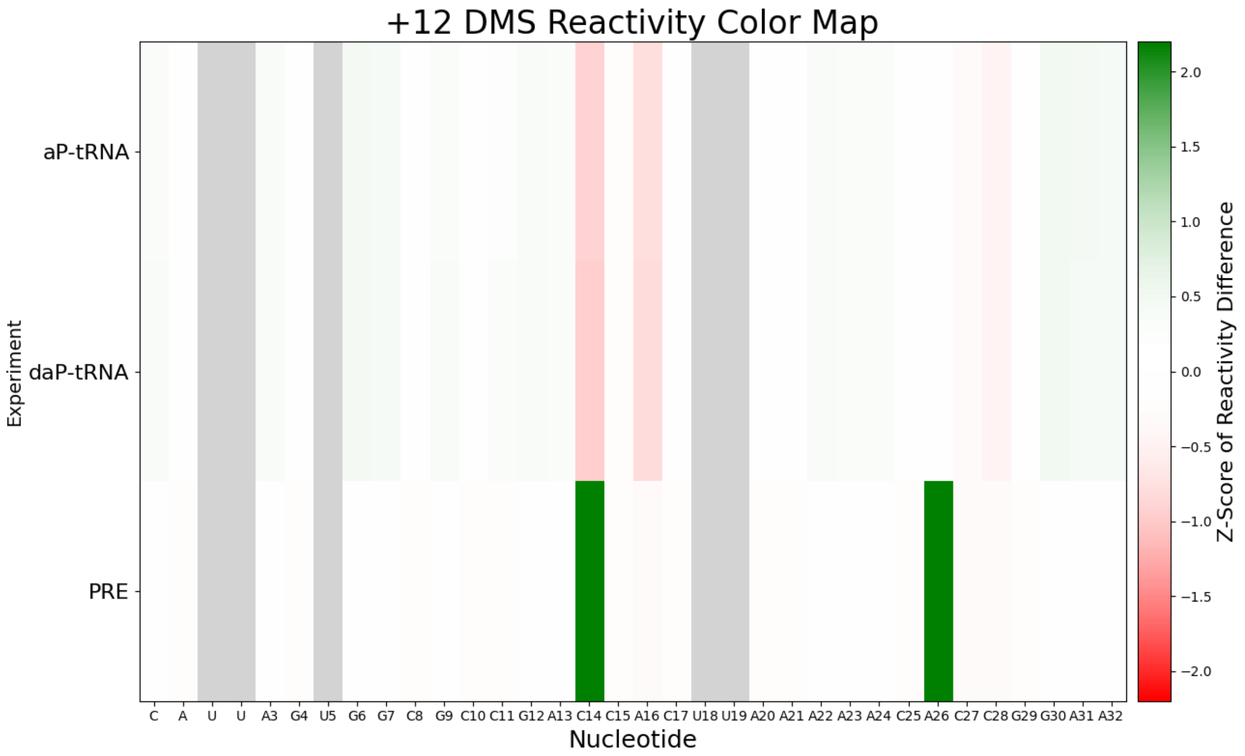
+12 DMS Reactivity Color Map
Experiment
aP-tRNA
daP-tRNA
PRE
C A U U A3 G4 U5 G6 G7 C8 G9 C10 C11 G12 A13 C14 C15 A16 C17 U18 U19 A20 A21 A22 A23 A24 C25 A26 C27 C28 G29 G30 A31 A32
Nucleotide
2.0
1.5
1.0
0.5
0.0
−0.5
−1.0
−1.5
−2.0
Z-Score of Reactivity Difference

Figure 4

A)

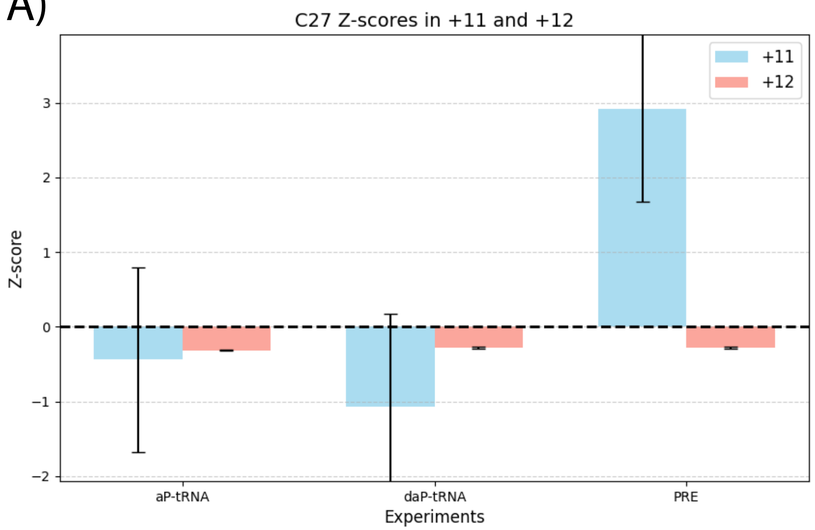
C27 Z-scores in +11 and +12
+11
+12
Z-score
3
2
1
0
−1
−2
aP-tRNA
daP-tRNA
PRE
Experiments

B)

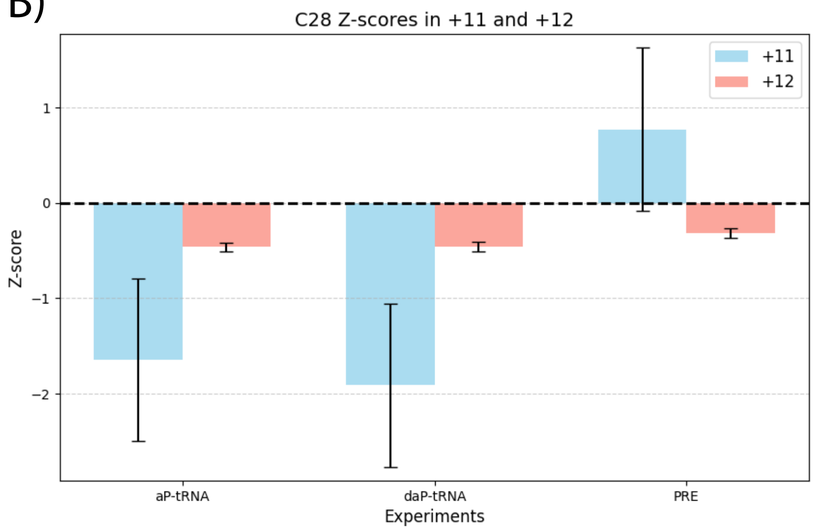
C28 Z-scores in +11 and +12
+11
+12
Z-score
1
0
−1
−2
aP-tRNA
daP-tRNA
PRE
Experiments

Figure 5

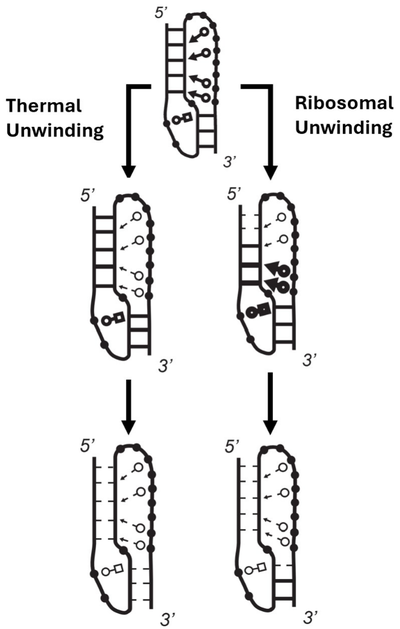

Figure 6